Christian Weber, Markus Tahedl, and Olfa Kanoun

Modeling for improved performance of non-contacting capacitive sensors for detecting aqueous solutions

Abstract: In industrial applications, non-contacting capacitive sensors are used to detect conductive fluids in containers. During use, the material to be detected can stick to the inside of the container, leading to measurement deviations. Using analytical modeling, it has been found that an overall resistance can distinguish between the conductive film and the actual fill level. Impedance analyzers have limitations with respect to their maximum measurement frequency of approximately 100 MHz. This bandwidth is not sufficient for characterizing highly conductive media. In order to overcome this limitation, improved signal processing is proposed to determine the overall resistance. In this paper, two methods of parameter extraction using the total measured bandwidth and a limited frequency range are compared. Results show that the overall resistance can be extracted using only a limited frequency range.

Keywords: impedance sensors, capacitive sensors, parameter extraction, modeling, impedance spectroscopy

1 Introduction

Limit levels of a container filled with a conductive fluid can be detected using capacitive sensors. For easy installation, the sensors are mounted outside of the non-conductive container. Conductive films inside of the container influence the sensor signal and can produce a false positive detection of the medium [1].

Fig. 1 shows a capacitive limit level switch mounted outside a container. Since in many applications the exact geometry, i. e., container material and wall thickness, and material properties of the medium are unknown, the sensors have to be calibrated before use. This is often done by adjusting the switch point using a potentiometer. Simple capacitive proximity switches measure only the absolute impedance between their sensing electrode and ground potential [2, 3]. Depending on the measurement frequency, wall thickness and conductivity of the fluid, the measured value of such sensors is the same for both the actual fill level and a conductive film.

Christian Weber, ifm electronic gmbh, Essen, Germany, e-mail: christian.weber@ifm.com
Markus Tahedl, Oertli Instrumente AG, Berneck, Switzerland
Olfa Kanoun, Chair for Measurement and Sensor Technology, Chemnitz University of Technology, Reichenhainer Strasse 70, 09126 Chemnitz, Germany

https://doi.org/10.1515/9783110558920-011

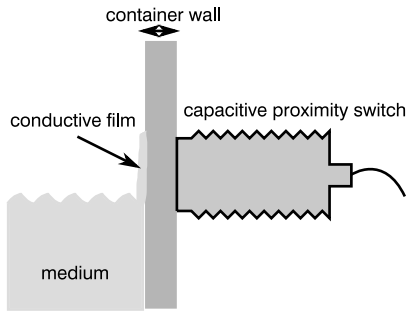

Fig. 1: Capacitive proximity switch mounted outside a container for detecting the limit level of the medium. Conductive films may stick to the inside of the container wall.

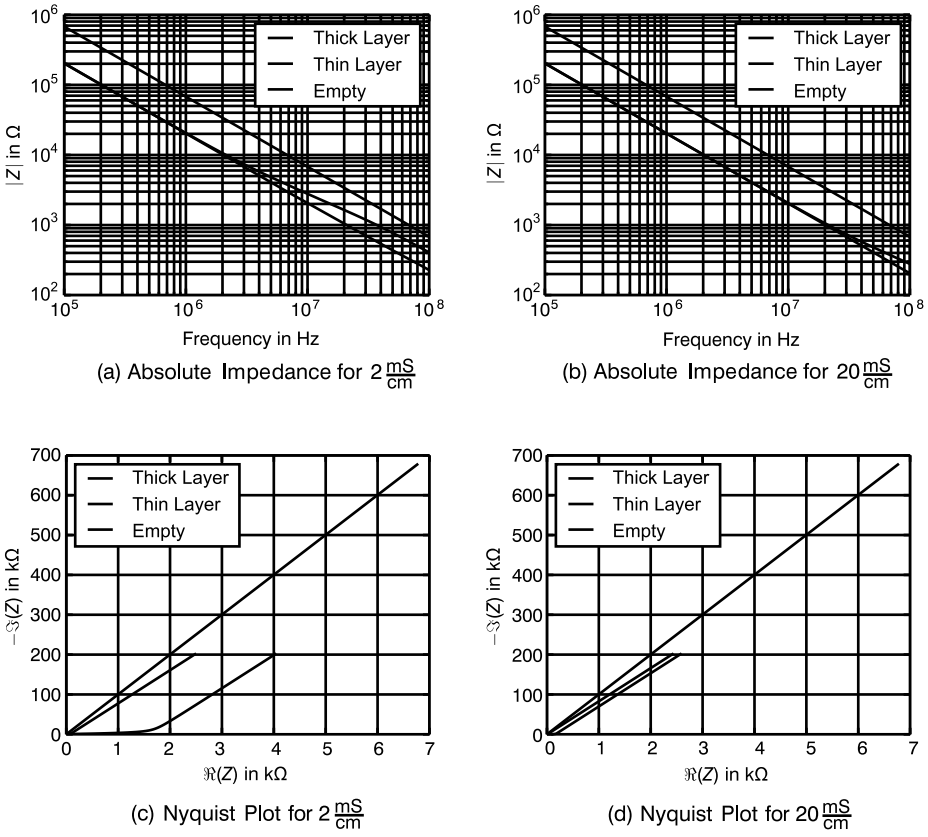

Fig. 2: Example plots to illustrate the difference between a thin layer and the actual full container for two different conductivities.

To illustrate the problem, Fig. 2 shows example spectra for a full container and a thin conductive film of a conductive aqueous solution for two conductivities 2 mS/cm and 20 mS/cm. It is shown in Fig. 2 (a) that a thin conductive film cannot be distinguished from the actual fill level below a frequency of 2 MHz. A difference between a thin and a

thick layer can only be observed at frequencies above 2 MHz. This effect is even worse at higher conductivities, as can be seen in Fig. 2 (b), where the difference between thin and thick layers is only observable at frequencies higher than 20 MHz. The necessary measurement frequency increases approximately proportionally with the conductivity of the material to be detected.

Fig. 3 shows the difference of the absolute impedance, $\Delta|Z| = |Z_{\text{thin}}| - |Z_{\text{thick}}|$, between a thin layer and a thick layer for several conductivities. It can be seen in the figure that the maximum difference decreases with increasing conductivity. Furthermore, the measurement frequency at which the maximum difference occurs also increases with conductivity.

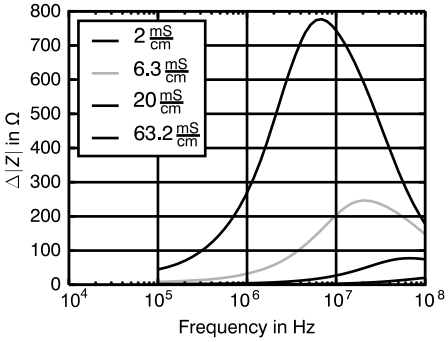

Fig. 3: Absolute difference $\Delta|Z| = |Z_{\text{thin}}| - |Z_{\text{thick}}|$ between a thin layer and a thick layer of the medium. Increasing the frequency reduces the observed difference and increases the necessary measurement frequency.

Since measurement devices are limited in terms of measurement frequency, another method must be found. Figs. 2 (c) and 2 (d) show complex Nyquist plots of the same dataset. It is possible to distinguish thin films and actual limit levels using impedance spectroscopy and associated signal processing techniques. The low-frequency part, where the Nyquist plot forms a straight line, can be shifted to the right by a decrease in layer thickness or a decrease in conductivity. Therefore, for a given conductivity, different layer thicknesses can be distinguished by inspection of the complex impedance plot even though there is no difference visible in the absolute value of the impedance.

Using analytical modeling, it was found that the overall resistances of a capacitively coupled aqueous solution can be used to distinguish between the conductive film and the actual limit level [1, 4]. To validate the proposed criterion experimentally, a measurement setup is needed to create thin layers of aqueous solutions.

This setup has already been described in [5]. However, the fitting methods are reported to have some limitations. Relative fitting errors of the proposed fitting procedures are quite large, up to 20 % in the real part of the measured spectrum.

In this contribution, improved fitting procedures are proposed to increase the quality of fit, which has been improved to below 0.5 % and 7 % for the imaginary and the real part, respectively. For very high conductivities, e. g., aqueous KCl solu-

tions with a conductivity of up to 208 mS/cm [6, 7], a linear fitting procedure [1] is introduced. In the next sections, we introduce and compare two fitting procedures.

For low solution conductivity, the parameters of a behavioral equivalent circuit model are extracted using differential evolution. For high solution conductivity, low-frequency data are fitted to a first-order polynomial and the overall resistance is determined.

2 Extraction of the overall resistance by non-linear fitting

To adequately model the behavior of measured and simulated impedance spectra, the electrical equivalent circuit (EEC) shown in Fig. 4 can be used.

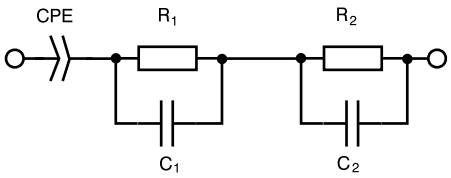

Fig. 4: Behavioral model for the complex impedance of capacitively coupled conductive media.

Since the electrode is mounted outside a non-conducting container, the capacitive coupling into the material under test (MUT) can be modeled using a constant phase element (CPE). Its impedance can be parameterized as follows [8]:

$$Z_{\mathrm{CPE}} = \frac{1}{K} \cdot (j\omega)^n, \tag{1}$$

where j is the imaginary unit and K denotes the amplitude of the CPE; n can be any real value between –1 and 1 and is a measure for the dielectric loss factor D. We have

$$D = \frac{\Re(Z)}{\Im(Z)}. \tag{2}$$

If $n = 0$, the CPE becomes an Ohmic resistance $R = \frac{1}{K}$. For $n = -1$, the equation yields an ideal capacitance $C = K$; $n = 1$ yields an inductance $L = \frac{1}{K}$.

To link n and D, we rewrite equation (1) using [8] and we obtain

$$Z_{\mathrm{CPE}} = \frac{\omega^n}{K} \cdot \left(\cos\left(n\frac{\pi}{2}\right) + j \cdot \sin\left(n\frac{\pi}{2}\right)\right). \tag{3}$$

Substituting into equation (2) yields

$$D = \frac{\cos(n\frac{\pi}{2})}{\sin(n\frac{\pi}{2})} = \frac{1}{\tan(n\frac{\pi}{2})}. \tag{4}$$

The equations for the CPE phase angle φ and quality factor Q are then

$$\varphi = n\frac{\pi}{2}, \tag{5}$$

$$Q = \frac{1}{D} = \tan\left(n\frac{\pi}{2}\right). \tag{6}$$

If an alternating electric potential is applied to an electrode, the equation of continuity of the electric current density states that the current can be separated into a dielectric and a conductive part [9]. Thus, the behavior of a conductive aqueous solution can be described by a series of resistor–capacitor (RC) elements. The impedance of a single RC element is

$$Z_{\mathrm{RC}} = \frac{R}{1 + j\omega RC}. \tag{7}$$

Substituting $\omega_{\mathrm{g}} = \frac{1}{\mathrm{RC}}$ yields

$$Z_{\mathrm{RC}} = \frac{R}{1 + j\frac{\omega}{\omega_{\mathrm{g}}}}. \tag{8}$$

Thus, the model impedance Z_{mod} is

$$Z_{\mathrm{mod}} = \frac{1}{K} \cdot (j\omega)^n + \frac{R_1}{1 + j\frac{\omega}{\omega_{\mathrm{g},1}}} + \frac{R_2}{1 + j\frac{\omega}{\omega_{\mathrm{g},2}}}. \tag{9}$$

To extract the model parameters of the EEC shown in Fig. 4, a differential evolution algorithm as proposed in [5] was used. Evolutionary algorithms benefit from a large search space and robust convergence behavior [10, 11]. Compared to gradient methods, which tend to get trapped in local minima of the cost function, especially at increased noise levels, stochastic methods are more robust because no gradients are calculated [12], though it is worth mentioning that the noise level of an optimization problem also depends on the cost function employed [13].

The first two points are of special interest here, since the impedance spectra of the EEC in question require a high-frequency bandwidth for all parameters to be extracted [5].

For the fitting procedure to succeed, a suitable cost function must first be defined. Since the measured data represent a capacitively coupled conductive fluid, the phase angle of the measured impedance is always relatively close to −90°. It is therefore not recommended to use the absolute difference between measured and modeled data as a cost function since it is mainly sensitive to changes in the imaginary part of the spectrum. Instead, we propose to adopt a parametric cost function c as proposed by [14] to describe the modeling error for N data points and M parameters, i. e.,

$$c = \frac{1}{N - M}\sum_{\mathrm{i}=1}^{N}\left(\frac{(\Re(Z_{\mathrm{i,meas}}) - \Re(Z_{\mathrm{i,mod}}))^2}{\Re(Z_{\mathrm{i,meas}})^2} + \frac{(\Im(Z_{\mathrm{i,meas}}) - \Im(Z_{\mathrm{i,mod}}))^2}{\Im(Z_{\mathrm{i,meas}})^2}\right). \tag{10}$$

This cost function describes the sum of relative quadratic residuals of the measured data. This way, the real and imaginary residuals at all frequencies contribute equally to the cost function, which allows for a better extraction of the unknown parameters. When using differential evolution, extracted parameters can depend on the parameter boundaries specified. Since model parameters must be found over a large frequency bandwidth and the algorithm should work on as many different spectra as possible, parameter boundaries also become very broad, ranging over several decades. Thus, we propose to employ logarithmic compression to shrink the search space, i. e.,

$$R_{\log} = \log_{10}\left(\frac{R}{1\Omega}\right). \tag{11}$$

For example, if the search space for a single resistance ranges from 1 Ω to 1 MΩ, one substitutes both of these values into equation (11), which yields unitless values of 0 and 6, respectively.

At low frequencies, the real and imaginary parts of an impedance spectrum of a capacitively coupled aqueous solution have a high sensitivity with respect to the CPE parameters [5]. Small perturbations in these parameters will cause a large fitting error. To guarantee a reliable extraction of the CPE parameters, we suggest to first estimate the CPE parameters from the measured data and then choose the initial population boundaries to be within ±50 % of the estimated values. The CPE values can be estimated by linearly fitting the low-frequency part of the spectrum to a first-order polynomial, i. e.,

$$\Re(Z) = D_{\mathrm{E}} \cdot \Im(Z) + R_{\mathrm{O}}. \tag{12}$$

Fig. 5 shows an illustration of the linear fitting procedure. For a successful estimation, the part of the Nyquist plot where the impedance curve forms a straight line must be used. The imaginary part of the spectrum is used as an independent variable; R_{O} is the intercept point with the real axis at $\Im(Z) = 0$. The loss factor D_{E} represents the slope of the low-frequency line.

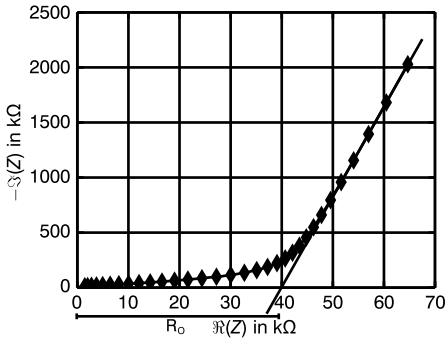

Fig. 5: Illustration of the estimation of overall resistance and CPE parameters.

Using equation (5), the exponent n_{ab} of CPE can be approximated; K can be approximated by rearranging equation (1), i. e.,

$$K_{ab} = \frac{1}{Z(\omega_1) - R_O} \cdot (j\omega_1)^{n_{ab}}, \tag{13}$$

where $Z(\omega_1)$ is the measured impedance at the lowest frequency. With the estimated CPE parameters and logarithmic compression for all RC elements, the initial population is computed using latin hypercube sampling [15]. After convergence of the differential evolution optimizer, the implementation [15] employed in this work can optionally refine the stochastic result with a direct search optimizer [16, 17]. If the direct search optimizer yields, in terms of cost, a better result than the evolution algorithm, its solution is replaced. If not, the result of the differential evolution is returned.

2.1 Evaluation of the proposed modifications

To evaluate the proposed method, a noiseless test dataset using the EEC shown in Fig. 4 is generated in a frequency range from 1 kHz to 100 MHz with the nominal values shown in Table 1. The modified extraction method with logarithmic compression and approximation of the CPE parameters was compared against a classical differential evolution approach. For both methods the algorithm was set up with the same population size of 80 individuals, 10^4 maximum iterations and the same convergence criterion described in [15]. The algorithm terminates if

$$\frac{\text{stdev (population)}}{\text{mean (population)}} < 10^{-3} \tag{14}$$

is true, where stdev (population) denotes the standard deviation of the population. All other parameters of the optimizer were left at the standard values provided by its implementation in the Python module Scipy 0.18 [15].

In the implementation used in this study, C_1 and C_2 are also treated as CPEs to make the algorithm easily expandable to more complex models, though their exponents n are chosen in such a way that their loss factor does not exceed 1.6×10^{-12}.

Table 1: Result of the parameter reconstruction.

Parameter	Nominal value	Modified reconstruction	Classical reconstruction
n	−0.9923	−0.9923	−0.9923
K in $\frac{1}{\Omega}(\frac{\text{rad}}{\text{s}})^n \cdot 10^{-12}$	4	4	4
C_1 in pF	150	149.99	10^4
C_2 in pF	14.5	14.5	13.2
R_1	500.00	500.00	999633.70
R_2	6600	6599.99	7086.71
Cost function c	0	2.61×10^{-20}	1.01×10^{-6}

The boundary values for the search space of the resistances is $[0, 6]$ (logarithmic) for the modified method and $[1\Omega, 1\,\mathrm{M}\Omega]$ for the classical method. For capacitances, intervals of $[-13, -8]$ (logarithmic) and $[10^{-13}\mathrm{F}, 10^{-8}\mathrm{F}]$ were chosen. For the coupling CPE, the modified method employs boundary values of $[0.5\times K_{\mathrm{ab}}, 1.5\times K_{\mathrm{ab}}]$ and $[-1, 0.9\times n_{\mathrm{ab}}]$, while the classical method uses $[10^{-13}\frac{1}{\Omega}(\frac{\mathrm{rad}}{\mathrm{s}})^n, 10^{-8}\frac{1}{\Omega}(\frac{\mathrm{rad}}{\mathrm{s}})^n]$ for the CPE amplitude and $[-1, -0.8]$ for the CPE exponent n. Implementation was done using [15, 18].

Table 1 shows that a reconstruction of the nominal parameters is possible with the proposed method. With the classical method, the algorithm seems to converge to a local minimum, as can be seen in the rightmost column of the table.

Furthermore, the result of the classical method is not always reproducible. Multiple optimization runs yield different parameter vectors with cost function values, which in some cases are as high as $c \approx 0.3$.

For the classical method to converge to the correct solution, the parameter boundaries have to be narrowed by two decades to $[10^{-12}\mathrm{F}, 10^{-9}\mathrm{F}]$ for the capacitances and $[1\Omega, 10\,\mathrm{k}\Omega]$ for the resistances. This shows that using logarithmic compression increases conversion reliability and user convenience.

However, at the chosen population size of 80 individuals, using linear fitting to estimate the CPE parameters does not seem to be necessary as long as logarithmic compression is used. The evolution algorithm also converges on the nominal parameter values even if the parameter boundaries for the coupling CPE are set to be $[10^{-13}\frac{1}{\Omega}(\frac{\mathrm{rad}}{\mathrm{s}})^n, 10^{-8}\frac{1}{\Omega}(\frac{\mathrm{rad}}{\mathrm{s}})^n]$ and $[-1, -0.8]$.

Although the linear parameter estimation does not yield significant improvement to the non-linear extraction, it is still useful to characterize solutions where the measured spectrum does not contain enough information about all RC elements.

3 Extraction of the overall resistance by linear fitting

Because of the limited measurement bandwidth, it is not always possible to extract all time constants of a given measured spectrum. However, one can still obtain information about the overall resistance and the coupling CPE. Instead of fitting the impedance spectrum over its full bandwidth, one can use equation (12), which is used to extract CPE parameters before a non-linear regression. It has already been shown experimentally in a previous work that this parameter is related to layer thickness and conductivity of the fluid [1]. Using a behavioral model with a CPE and one RC element with time constant $\tau = R_1C_1$, it can be shown that R_0 is an approximation of R_1. Most symbolic calculations have been carried out using [19]. Separation of real and imaginary part of the impedance yields

$$\Re(Z) = \frac{1}{K(C_1^2R_1^2\omega^2 + 1)}\left(C_1^2R_1^2\omega^{n+2}\cos\left(\frac{\pi n}{2}\right) + KR_1 + \omega^n\cos\left(\frac{\pi n}{2}\right)\right), \tag{15}$$

$$\mathfrak{I}(Z) = \frac{1}{K(C_1^2R_1^2\omega^2+1)}\left(C_1^2R_1^2\omega^{n+2}\sin\left(\frac{\pi n}{2}\right) - C_1KR_1^2\omega + \omega^n\sin\left(\frac{\pi n}{2}\right)\right). \tag{16}$$

In the frequency region where the Nyquist plot forms a straight line, two frequencies ω_1 and ω_2 are selected. The line slope D_E can be approximated as follows:

$$D_\mathrm{E}(\omega_1,\omega_2) = \frac{\Re(Z(\omega_1)) - \Re(Z(\omega_2))}{\mathfrak{I}(Z(\omega_1)) - \mathfrak{I}(Z(\omega_2))}. \tag{17}$$

By substituting equation (17) into equation (12) and solving for R_O we get

$$R_\mathrm{O}(\omega_1,\omega_2) = \Re\big(Z(\omega_1)\big) - D_\mathrm{E}(\omega_1,\omega_2)\cdot\mathfrak{I}\big(Z(\omega_1)\big). \tag{18}$$

We now let the difference between the two frequencies approach zero by calculating the limit, i. e.,

$$R_\mathrm{O}(\omega_2) = \lim_{\omega_1\to\omega_2} R_\mathrm{O}(\omega_1,\omega_2), \tag{19}$$

and we get

$$R_\mathrm{O}(\omega_2) = \frac{R_1\left(\frac{C_1R_1\omega_2}{\tan\left(\frac{\pi n}{2}\right)}+1\right)}{C_1^2R_1^2\omega_2^2+1}. \tag{20}$$

For simplicity, we also substitute $R_1C_1 = \frac{1}{\omega_\mathrm{g}}$, so we obtain

$$R_\mathrm{O}(\omega_2) = \frac{R_1}{\frac{\omega_2^2}{\omega_\mathrm{g}^2}+1}\left(\frac{\omega_2}{\omega_\mathrm{g}\tan\left(\frac{\pi n}{2}\right)}+1\right). \tag{21}$$

Equation (21) has a pole for $n = 0$. However, this pole is not relevant in the application discussed here, because the CPE becomes a pure resistance in that case, thus removing the capacitive coupling from the system; R_O is a good approximation of R_1, if $\omega_\mathrm{g} \gg \omega_2$ holds. In this case, the terms $\frac{\omega_2^2}{\omega_\mathrm{g}^2}$ and $\frac{\omega_2}{\omega_\mathrm{g}\tan\left(\frac{\pi n}{2}\right)}$ both approach zero and the equation becomes $R_\mathrm{O} = R_1$. Typically, $\omega_\mathrm{g} \gg \omega_2$ is fulfilled for highly conductive media since the low resistances cause high cut-off frequencies.

It can also be shown that D_E is a good approximation for the impedance loss factor D. The loss factor of an EEC containing one RC element and one CPE is

$$D = \frac{\frac{KR_1}{\frac{\omega^2}{\omega_\mathrm{g}^2}+1} + \frac{\omega^2\omega^n\cos\left(\frac{\pi n}{2}\right)}{\omega_\mathrm{g}^2\left(\frac{\omega^2}{\omega_\mathrm{g}^2}+1\right)} + \frac{\omega^n\cos\left(\frac{\pi n}{2}\right)}{\frac{\omega^2}{\omega_\mathrm{g}^2}+1}}{-\frac{KR_1\omega}{\omega_\mathrm{g}\left(\frac{\omega^2}{\omega_\mathrm{g}^2}+1\right)} + \frac{\omega^2\omega^n\sin\left(\frac{\pi n}{2}\right)}{\omega_\mathrm{g}^2\left(\frac{\omega^2}{\omega_\mathrm{g}^2}+1\right)} + \frac{\omega^n\sin\left(\frac{\pi n}{2}\right)}{\frac{\omega^2}{\omega_\mathrm{g}^2}+1}}. \tag{22}$$

If $\omega_\mathrm{g} \gg \omega$ holds, we can calculate the limit, i. e.,

$$D_\mathrm{E} = \lim_{\frac{\omega}{\omega_g}\to 0} D = \frac{\omega^{-n}}{\sin\left(\frac{\pi n}{2}\right)}\left(KR_1 + \omega^n\cos\left(\frac{\pi n}{2}\right)\right), \tag{23}$$

which we can write as

$$D_E = \frac{\omega^{-n} K R_1}{\sin(\frac{n\pi}{2})} + \frac{\cos(\frac{n\pi}{2})}{\sin(\frac{n\pi}{2})}. \tag{24}$$

The denominator of the first additive term of equation (24) is close to –1 since n is also close to –1 for a capacitively coupled medium. Also, $\omega^{-n} \approx \omega$ holds for the same reason. However, since K is typically small, approximately $10^{-12}\,\frac{1}{\Omega}(\frac{\mathrm{rad}}{\mathrm{s}})^n$ to $10^{-10}\,\frac{1}{\Omega}(\frac{\mathrm{rad}}{\mathrm{s}})^n$, it can be stated that for small values of R_1 the first additive term approaches zero. Thus, D_E approaches D.

Equations (21) and (24) show that a linear fitting routine can be used to extract the two CPE parameters and the overall resistance R_O, which is closely related to the actual resistance of the fluid. Therefore, even though the bandwidth of the measurement setup is limited, it can still be used to characterize highly conductive media.

4 Experimental investigations

The proposed fitting methods are now validated using measured data. The media and conductivities used are listed in Table 2.

Table 2: Conductivity of the measured media.

Medium	Conductivity σ in mS/cm
Tap water	0.5
KCl #1	1.9
KCl #2	10.6
KCl #3	43.1
KCl #4	92.5
KCl #5	193.1

Fig. 6 shows a concept drawing of the proposed measurement setup. It consists of an outer and an inner cylinder fabricated from plastic. The inner cylinder is hollowed out to minimize its influence of the measured impedance. Its height can be adjusted to create a defined gap at the bottom of the setup, where the measurement electrode is mounted. The height of this gap will be referred to as layer thickness. The aqueous solution to be measured is inserted between the outer and the inner cylinder. A detailed description is available in [2]. Impedance spectra were recorded at 801 frequency points, the maximum amount for a single sweep, in a range from 4 kHz to 110 MHz.

Measurement noise of the impedance measurement instrument depends on various factors, i. e., the connected device under test, the selected frequency range and

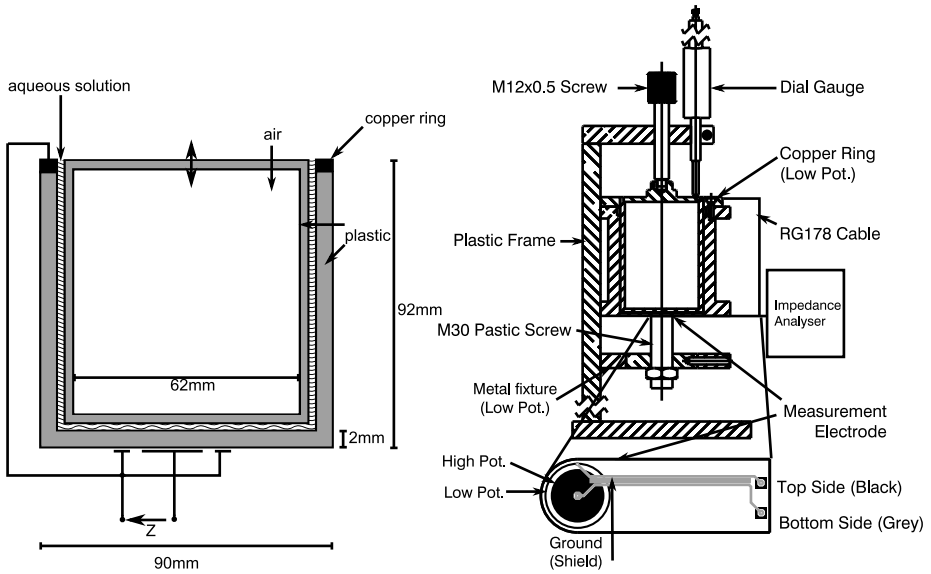

Fig. 6: Measurement setup drawings [5]. The setup is connected to an impedance measurement instrument, which provides high, low and ground potential terminals.

the test signal level [3]. Measurement noise for capacitively coupled resistances characterized in this work was approximated by connecting an inter-digital capacitor on an FR4 printed circuit board with CPE values $K = 5.7 \times 10^{-12} \frac{1}{\Omega} (\frac{\text{rad}}{\text{s}})^n$ and $n = -0.99$ connected in series to a 150-Ω resistor. A total of 600 spectra with 50 points each in a frequency range from 1 MHz to 5 MHz were recorded. The maximum relative standard deviations for the absolute impedance and its phase angle are 0.07 % and 0.007 %, respectively.

Measured data are smoothed using a linear fitting algorithm [21] with the modifications described in [1, 22, 23]. For all models, the relative residuals for real Δ_{re} and imaginary Δ_{im} part of the impedance are calculated as follows:

$$\Delta_{\text{re}} = \frac{\Re(Z_{\text{meas}}) - \Re(Z_{\text{mod}})}{\Re(Z_{\text{meas}})} \cdot 100\,\%, \tag{25}$$

$$\Delta_{\text{im}} = \frac{\Im(Z_{\text{meas}}) - \Im(Z_{\text{mod}})}{\Im(Z_{\text{meas}})} \cdot 100\,\%, \tag{26}$$

where Z_{meas} denotes the measured impedance while Z_{mod} is the modeled impedance. A measured impedance is excluded from the spectrum, if its relative residual in either the real or the imaginary part exceeds 0.5 %. However, even though the fitting procedure itself is optimized, the selection of error thresholds and frequency bandwidth

must still be done by the user. Therefore, different media can have different frequency ranges.

4.1 Extraction by non-linear fitting

The filtered spectra for tap water and KCl #1 are then used to validate the improved fitting procedure. All other media are employed to validate the linear fitting method, since sensitivity analyses have shown [5] that the measurement bandwidth for high conductivities is insufficient to extract all parameters of the EEC. Fig. 7 shows the relative residuals for tap water and KCl #1. A series inductance L_s has been added to the EEC to model the influence of cables connected to the measurement setup. This significantly reduces the relative residual in the imaginary part for frequencies greater than 10 MHz. The relative error of the imaginary part, shown in Figs. 7 (d) and 7 (c), is now below 0.5 %. The extracted value does not change over varying layer thickness

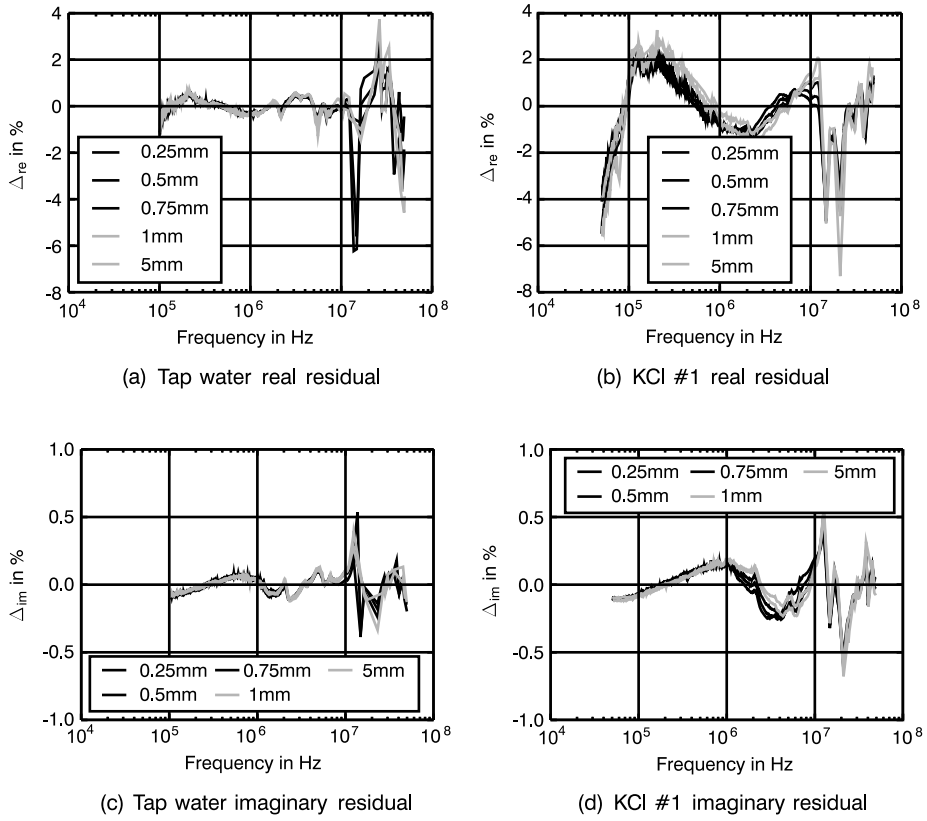

Fig. 7: Relative residuals after non-linear fitting for tap water and KCl #1.

and changes by about 10 nH, when the MUT conductivity is increased. This suggests that L_s can be solely attributed to the measurement setup itself.

The maximum residual observed for Δ_{re} is 7 %, which is a significant improvement in comparison to [5], where the maximum fitting error in the real part is up to 20 %. Significant errors arise for frequencies below 100 kHz and above 10 MHz. At lower frequencies, the measured spectrum is dominated by the CPE and small changes to its parameters cause a significant change in the modeled impedance, as can be seen in Fig. 8. Also measured signals in this region are very small, causing a decrease in the measurement accuracy, especially in $\Re(Z_{meas})$ [20].

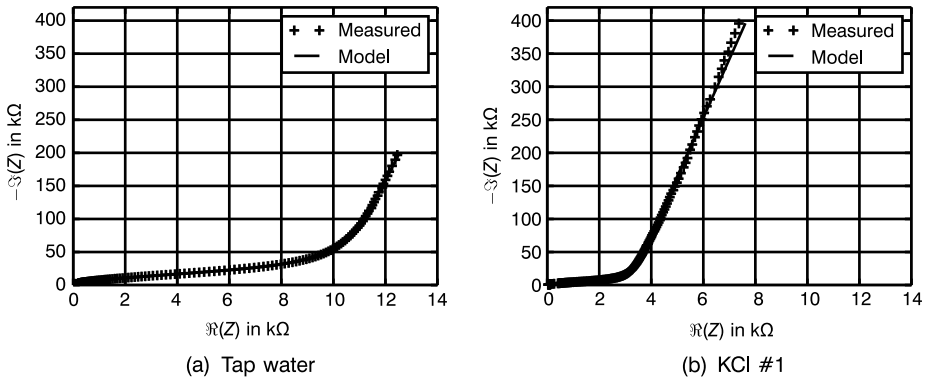

Fig. 8: Example plots of measured and fitted data for a layer thickness of 0.25 mm. For visibility reasons, only every third measurement point is shown.

Since all frequencies have an equal weight in the employed cost function, measurement errors in this region contribute equally to the fitted parameters. If frequencies below 100 kHz are excluded, Δ_{re} is below 1 % for frequencies between 100 kHz and 10 MHz, as can be seen in Fig. 7 (a). Above 10 MHz high relative residuals are observed at single measurement points. These might be caused by electromagnetic coupling into the measurement setup. Since the data smoothing is based on a linear fit, it minimizes the weighted quadratic sum of residuals, which might allow single points to pass through the smoothing scheme. To further increase accuracy, it is feasible to first extract parameters over a broad smoothed spectrum and then exclude frequency ranges with a high relative residual.

Tables 3 and 4 show the extracted values. As expected, the CPE parameters K and n do not depend on layer thickness and conductivity. Their maximum deviation is 1.72 % and 0.08 % and therefore they only represent the capacitive coupling into the MUT. Resistances decrease monotonously with increasing layer thickness and conductivity. Resistances decrease with layer thickness because of the increasing cell constant. For constant geometries the sum of R_1 and R_2 is in good approximation inversely proportional to the MUT conductivity; C_1 and C_2 increase monotonously with increasing layer

Table 3: Parameters extracted by non-linear fitting for KCl #1 for several layers.

Parameter	0.25 mm	0.5 mm	0.75 mm	1 mm	5 mm
n	−0.9928	−0.9927	−0.9926	−0.9926	−0.9927
K	$8.77 \cdot 10^{-12}$	$8.77 \cdot 10^{-12}$	$8.78 \cdot 10^{-12}$	$8.78 \cdot 10^{-12}$	$8.78 \cdot 10^{-12}$
C_1 in pF	62.0	65.1	71.1	82.9	142.0
C_2 in pF	13.0	13.8	15.0	15.3	17.1
R_1 in Ω	165.72	126.44	97.41	73.24	51.76
R_2 in Ω	2982.90	2446.66	2076.06	1980.07	1651.90
L_s in nH	251	249	249	246	251

Table 4: Parameters extracted by non-linear fitting for tap water for several layers.

Parameter	0.25 mm	0.5 mm	0.75 mm	1 mm	5 mm
n	−0.9923	−0.9922	−0.9923	−0.9922	−0.9924
K	$8.87 \cdot 10^{-12}$	$8.83 \cdot 10^{-12}$	$8.81 \cdot 10^{-12}$	$8.82 \cdot 10^{-12}$	$8.86 \cdot 10^{-12}$
C_1 in pF	77.8	77.2	80.5	81.9	167.0
C_2 in pF	12.7	13.5	14.8	15.2	17.1
R_1 in Ω	319.28	290.71	234.67	228.05	84.55
R_2 in Ω	9868.40	8318.83	6892.72	6806.33	6060.37
L_s in nH	235	240	238	236	234

thickness. This behavior can be expected because the mean permittivity increases when more water is present in the setup.

4.2 Extraction by linear fitting

In the previous section, broadband characterization has been used to extract all system parameters including the overall resistances. However, this approach fails for high conductivities because of insufficient sensitivity of the RC elements. The linear fitting procedure is independent of this sensitivity. Accuracy of the extracted CPE parameters can also be increased using the linear fitting method, because it only utilizes a measurement bandwidth, where the impedance spectrum is dominated by the CPE and the overall resistance.

Thus, for all other media the overall resistances are extracted using the linear fitting procedure. Results are shown in Table 5. Just like the resistances obtained with the non-linear fitting procedure, extracted values decrease monotonously with layer thickness and conductivity. Also, the sensitivity of R_0 with respect to layer thickness decreases with increasing conductivity. This is consistent with modeling expectations formulated in [1]. For KCl #5, the sensitivity becomes small and therefore susceptible

Table 5: Extracted R_0 values.

Layer thickness	Tap water	KCl #1	KCl #2	KCl #3	KCl #4	KCl #5
0.25 mm	10465.03	3110.23	652.22	165.58	62.06	22.32
0.5 mm	8906.57	2562.32	484.37	115.95	52.42	28.17
0.75 mm	7436.25	2174.59	391.52	94.89	42.82	23.66
1 mm	7341.06	2065.30	377.92	89.09	40.56	22.32
5 mm	6442.48	1719.78	319.35	72.12	33.34	19.40

to fitting errors caused by measurement noise. This can be circumvented by averaging over several spectra.

For tap water and KCl #1 the extracted R_0 values are within reasonable tolerances equal to the sum of R_1 and R_2 obtained by the non-linear fit. The maximum error for tap water is 4.8 % while the maximum error for KCl #1 is 1.2 %. This is in line with the predictions made in Section 3.

Also the relative change of the R_0 values for a constant layer thickness is approximately proportional to the change in conductivity, i. e., if the conductivity at 0.5 mm decreases by 30 % the R_0 value increases by about 30 %. The mean deviation from this proportionality is 8.2 % while the maximum deviation is about 33 % for KCl #5 at a layer thickness of 0.25 mm. A possible cause for this is the mechanical tolerance of the measurement setup, especially at small layer thicknesses.

4.3 Comparison of the two fitting methods

Fig. 9 illustrates the difference between the two fitting procedures. The non-linear fitting method employs the entire available frequency range, the full width of the Nyquist plot, to extract the parameters of the EEC shown in Fig. 4. However, for high conductivities the non-linear extraction fails, because of the short time constants formed by low resistances.

Using linear fitting on a limited frequency range, where the Nyquist plot is a straight line, one can still obtain the CPE parameters and the overall resistances R_0 and use them to distinguish between a thin film and the actual fill level, even though the non-linear fitting method fails due to insufficient sensitivity with respect to the RC elements.

In the previous sections, it has been shown mathematically and experimentally that R_0 is related to the resistances of the EEC.

Qualitative behavior of the extracted parameters is within theoretical expectations. However, the linear fit is only valid if the frequencies used for fitting are much smaller than the cut-off frequencies formed by the conductive and capacitive part of the current. This is usually the case for highly conductive media, for which this method is intended.

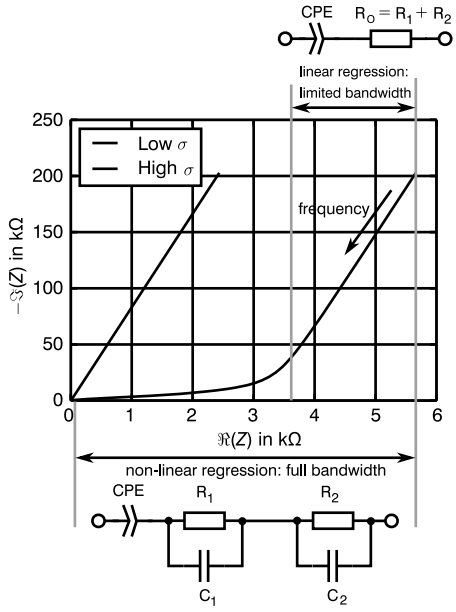

Fig. 9: Comparison of the two fitting methods. The non-linear regression utilizes the full measurement bandwidth and provides all model parameters, but fails if the bandwidth is insufficient. The linear regression utilizes only a limited portion of the measurement bandwidth but can be used even for highly conductive media, since the low-frequency information is always available.

5 Conclusion

Improved techniques for data processing have been proposed for measurement setups used to characterize thin layers of aqueous solutions. In contrast to [2], where fitting was done using purely gradient-based or direct search methods, broadband fitting of measured data to an EEC is now done using differential evolution and logarithmic compression of the parameter space.

Using differential evolution with logarithmic compression has been shown to increase reliability of conversion. The evolution algorithm can be called with larger search spaces, thus improving convenience for the user.

Also, a series inductance is introduced into the model to improve quality of fit at frequencies greater than 10 MHz. The improved method yields maximum relative errors of 0.6 % and 7 % in the imaginary and real parts of the spectrum, respectively. This is a significant improvement with respect to [5], where relative errors in the real part of the impedance were reported to be up to 20 %.

If characterization using linear fitting is sufficient, solutions with a conductivity of up to 190 mS/cm can be characterized.

Bibliography

[1] C. Weber, M. Tahedl, and O. Kanoun, “A novel method for capacitive determination of the overall resistance of an aqueous solution”, In: Progress Reports on Impedance Spectroscopy, De Gruyter, 2016.

[2] T. Grosse-Puppendahl, E. M. Berlin, and M. Borazio, “Enhancing accelerometer based activity recognition with capacitive proximity sensing”, In: A Nov Joi Conference on Ambient Intelligence, Springer, 2012, pp. 17–32.
[3] B. Osoinach, “Proximity capacitive sensor technology for touch sensing applications”, Freescale White Paper, vol. 12, 2007.
[4] C. Weber, F. Wendler, M. Tahedl, et al., “2d-modellierung des einflusses leitfähiger schichten auf die sensorimpedanz bei kapazitiven sensoren”, Tm - Technisches Messen, vol. 81, no. 9, pp. 442–449, 09/2014.
[5] C. Weber, M. Tahedl, and O. Kanoun, “Capacitive measurement setup for characterizing thin layers of aqueous solutions”, In: Progress Reports on Impedance Spectroscopy, Chemnitz, Germany, De Gruyter, 2016.
[6] R. Shreiner and K. Pratt, “Standard reference materials: Primary standards and standard reference materials for electrolytic conductivity”, NIST Special Publication, vol. 260, p. 142, 2004.
[7] W. Haynes, CRC Handbook of Chemistry and Physics, 93rd edition, CRC Handbook of Chemistry and Physics, Taylor & Francis, 2012.
[8] J. R. Macdonald, “Note on the parameterization of the constant-phase admittance element”, Solid State Ionics, vol. 13, pp. 147–149, 1984.
[9] H. Henke, ed. “Elektromagnetische Felder”, Springer, 2007.
[10] R. Storn and K. Price, “Differential evolution – a simple and efficient heuristic for global optimization over continuous spaces”, Journal of Global Optimization, vol. 11, pp. 341–359, 1997.
[11] O. Kanoun, U. Tröltzsch, and H.-R. Tränkler, “Benefits of evolutionary strategy in modeling of impedance spectra”, Electrochimica Acta, vol. 51, no. 8–9, pp. 1453–1461, 2006, Electrochemical Impedance Spectroscopy Selection of papers from the 6th International Symposium (EIS 2004), 16–21 May 2004, Cocoa Beach, FL, USA.
[12] T. VanderNoot and I. Abrahams, “The use of genetic algorithms in the non-linear regression of immittance data”, Journal of Electroanalytical Chemistry, vol. 448, no. 1, pp. 17–23, 1998.
[13] B. L. Miller and D. E. Goldberg, “Genetic algorithms, tournament selection, and the effects of noise”, Complex Systems, vol. 9, no. 3, pp. 193–212, 1995.
[14] A. S. Bondarenko and G. Ragoisha, “Potentiodynamic electrochemical impedance spectroscopy”, In: A. L. Pomerantsev, ed., Electrochimica Acta , Nova Science Publ, 2005, pp. 89–102.
[15] E. Jones, T. Oliphant, P. Peterson, et al., SciPy 0.18: Open source scientific tools for Python, 2001.
[16] C. Zhu, R. Byrd, and J. Nocedal, “L-bfgs-b: Algorithm 778: L-bfgs-b, fortran routines for large scale bound constrained optimization”, ACM Transactions on Mathematical Software, vol. 23, no. 4, pp. 550–560, 1997.
[17] R. Byrd, P. Lu, and J. Nocedal, “A limited memory algorithm for bound constrained optimization”, SIAM Journal on Scientific and Statistical Computing, vol. 16, no. 5, pp. 1190–1208, 1995.
[18] S. van der Walt, S. C. Colbert, and G. Varoquaux, “The numpy array: A structure for efficient numerical computation”, Computing in Science & Engineering, vol.. 13, no. 2, pp. 22–30, 03/2011.
[19] SymPy Development Team, Sympy: Python library for symbolic mathematics, 2016.
[20] Keysight Technologies, Keysight 4294a operation manual, Internet, Oktober 2016.
[21] B. A. Boukamp, “A linear Kronig–Kramers transform for immitance data validation”, Journal of the Electrochemical Society, vol. 142, no. 6, pp. 1885–1894, 1995.

[22] M. Schönleber, D. Klotz, and E. Ivers-Tiffée, "A method for improving the robustness of linear kramers-kronig validity tests", Electrochimica Acta, vol. 131, pp. 20–27, 2014, Electrochemical Impedance Spectroscopy.
[23] U. Tröltzsch, "Modellbasierte zustandsdiagnose von gerätebatterien", PhD thesis, Universität der Bundeswehr München, 2005.